Atomistic modelling of electron propagation and radiation emission in oriented bent ultra-thin Si and Ge crystals

V. V. Haurylavets[1], V. K. Ivanov[2], A. V. Korol[3], and A. V. Solov'yov[3]

[1]Research Institute for Nuclear Problems, Belarusian State University, Bobruiskaya street, 11, Minsk 220030, Belarus

[2]Peter The Great St.Petersburg Polytechnic University, Polytekhnicheskaya 29, St Petersburg, 194251, Russia

[3]MBN Research Center, Altenhöferallee 3, 60438 Frankfurt am Main, Germany

Abstract. Computational modelling of passage of high-energy electrons through crystalline media is carried out by means of the relativistic molecular dynamics. The results obtained are compared with the experimental data for 855 MeV electron beam incident on oriented bent ultra-thin (15 microns) silicon and germanium crystals. The simulations have been performed for the geometries of the beam–crystal orientation that correspond (i) to the channeling regime and (ii) to the volume reflection. A comparison with the experiment is carried out in terms of angular distributions of the electrons deflected by the crystals bent with different curvature radii as well as of the spectra of the emitted radiation. For both crystals a good agreement between the simulated and experimentally measured data is reported. The origin of remaining minor discrepancies between theory and experiment is discussed.

1. Introduction

The passage of a charged particle through a crystalline environment depends largely on the orientation of the particle's momentum and a crystallographic direction. Lindhard has demonstrated [1] that regularity in the atomic positions in a crystal can result in a specific channeling motion when a particle moves along a crystallographic plane or axis experiencing correlated interactions with the atoms. Since then, the passage of beams of ultra-relativistic charged particles through oriented crystals (channeling phenomenon included) has become a broad field of research [2, 3]. The knowledge acquired in theoretical and experimental investigations has led to a number of applications, either already implemented or potential ones, the realisation of which requires further efforts. Examples of the former include beam steering [4–6], collimation [7], focusing [8], and extraction [2]. Oriented crystals of different geometries (linear, bent, periodically bent) exposed to the beams of ultra-relativistic electrons and positrons can potentially serve as novel intensive gamma-ray crystal-based light sources (CLS) operating in the MeV-GeV

photon energy range [9–11]. In addition to the channeling radiation [12], the particles channeling in bent crystals can emit synchrotron-like radiation due to the circular motion along the bent planes [13, 14]. Motion along periodically bent planes gives rise to the intensive undulator-type radiation [15, 16]. To a great extent, intensity of the radiation and, consequently, characteristics of CLS (number of photons, brilliance), depend on the magnitude of the so-called dechanneling length L_d, i.e., the average distance over which a particle moves in the channeling mode of motion before it leaves the channel due to uncorrelated collisions with atoms (the dechanneling process). In turn, L_d is determined by the energy and charge of the projectile particle, crystal orientation, and type of crystal atoms, and bending curvature (see, e.g., a review paper [17]). This parameter, which characterizes channeling efficiency, can be measured experimentally and/or calculated by means of accurate simulations of particles' passage through oriented crystals.

In recent years, a series of experiments has been carried out at different accelerator facilities aimed at investigating channeling and radiation emission phenomena in linear [18], bent [4, 6, 19–25], and periodically bent crystals [26–29].

In this paper, we present an independent analysis of the passage of ultra-relativistic electrons through oriented thin silicon and germanium crystals and of the emitted radiation. The analysis is based on the results of simulations performed within the framework of relativistic classical molecular dynamics by means of the MBN EXPLORER software package [30–32] and a supplementary special multitask software toolkit MBN STUDIO [33]. The results obtained are compared to the experimental data on angular distributions of electrons after passing through silicon and germanium crystalline targets presented in Ref. [23] and on the measured emission spectra taken from Ref. [25]. Both experiments were carried out at the MAinzer MIcrotron (MAMI) facility with a 855 MeV electron beam. The facility generates highly collimated beam so that in the simulations its angular divergence has been ignored. The beam was incident on thin silicon and germanium bent crystals. The crystals used were of high quality with a very low concentration of defects. By means of a specially designed holder [34] the same crystalline sample was bent remotely to achieve different bending curvatures. Beyond the target, the electrons were deflected by magnets and thus separated from the emitted photons. This allowed one to measure the angular distributions along with the emission spectra. More details on the experimental setup are given in Ref. [35].

In Section 2, we overview the methodology utilized to carry out the simulations. The parameters of the targets as well as the beam-crystal alignments used in the experiments are described in Section 3. In Section 4, the numerical results obtained are compared with the experimental data collected at MAMI. Section 5 summarizes the conclusions of this work and presents future perspectives.

2. Methodology

In this paper the method of relativistic classical molecular dynamics [36], implemented in the MBN EXPLORER package [30–33], is employed to model the motion of

charged ultra-relativistic particles in an electrostatic field of the crystalline medium. This approach implies generation of a large number N of statistically independent trajectories of projectile particles that can be analyzed further to carry out quantitative characterization of the particles' motion as well as of the radiation emitted.

To model the motion an ultra-relativistic particle of mass m, charge q and energy ε in an atomic environment, the following relativistic equations of motion are integrated numerically:

$$\dot{\mathbf{r}} = \mathbf{v}, \qquad \dot{\mathbf{v}} = \frac{q}{m\gamma} \left(\mathbf{E} - \frac{\mathbf{v}\,(\mathbf{E} \cdot \mathbf{v})}{c^2} \right) \tag{1}$$

where $\mathbf{r} = \mathbf{r}(t)$ and $\mathbf{v} = \mathbf{v}(t)$ are the instantaneous position vector and velocity of the projectile particle, $\gamma = \varepsilon/mc^2$ denotes the relativistic factor. The electric field at point $\mathbf{r}$ is calculated as $\mathbf{E} = -\boldsymbol{\nabla}\phi(\mathbf{r})$ with $\phi(\mathbf{r})$ standing for the field's potential. This quantity is calculated as the sum of potentials of individual atoms located at points $\mathbf{r}_i$:

$$\phi(\mathbf{r}) = \sum_i \phi_{\text{at}}\left(|\mathbf{r} - \mathbf{r}_i|\right) . \tag{2}$$

The atomic potentials can be computed within the frameworks of the approximations due to Moliére [37] and Pacios [38]. The latter is based on the solutions of the Hartree-Fock equations, therefore, it is more accurate especially at distances larger than the average atomic radius that can be estimated as the Thomas-Fermi radius a_{TF}. At distances less than a_{TF} both approximations provide the same result in contrast to frequently used Doyle-Turner scheme [39]. A comparative analysis of the atomic and interplanar potentials for Si an Ge calculated within the frameworks of these approximations is presented in Section Appendix A.

For a neutral atom, the potential $\phi(\mathbf{r})$ decreases rapidly at the distances $r \gg a_{\text{TF}}$. Therefore, at each step of integration of the equations of motion (1), the sum in (2) can be truncated by accounting only for those atoms that are located inside the sphere of a specified cut-off radius ρ with the center at $\mathbf{r}$. Typically, ρ is chosen to be tens times larger than the average atomic radius. The search for such atoms is carried out by means of the linked cell algorithm implemented in the MBN EXPLORER package. In the course of particle's passage through a crystal, the crystalline environment around the particle is generated by means of a dynamic simulation box which moves following the particle. Inside the box, the nodal positions are generated in accordance with the crystal lattice and accounting for the transformations that modify the structure to achieve desired geometry of the crystal (e.g., linear, bent, periodically bent crystals). The positions of the atoms are generated accounting for random displacement from the nodes due to thermal vibrations. More detailed description on the algorithms used to compute the trajectories at various scales, including macroscopically large ones, are presented in Refs. [17, 30, 31, 36].

To calculate a trajectory, the values of the transverse coordinates and velocities at the crystal entrance are generated randomly accounting for the crystal orientation with respect to the incident beam and for the beam emittance and size. Allowing also for randomness in positions of the lattice atoms due to thermal vibrations, one concludes

that each trajectory corresponds to a unique crystalline environment. Therefore, all simulated trajectories are statistically independent and can be analyzed further to quantify the process of interest. For each trajectory simulated the spectral distribution $\underset{.}{E}_j$ of the radiant energy emitted within a specified cone along the incident beam can be evaluated numerically following the procedure described in detail in Ref. [36]. To calculate the total emission spectrum (per particle) one averages $\underset{.}{E}_j$ over all trajectories: $\underset{.}{E} = N^{-1}\sum_{j=1}^{N}\underset{.}{E}_j$, where N is the number of trajectories.

The simulations have been performed for 855 MeV electrons passing through bent single silicon and germanium crystals. We aimed at quantitative description of orientational effects (channeling, volume reflection) that reveal themselves in angular distributions of deflected particles as well as in the spectra of emitted radiation. The dependencies of the distributions and the spectra on the atomic number Z of the target and on the curvature radius R have been investigated. Both crystals have the diamond cubic crystal structure but differ significantly in the atomic number: $Z_{\mathrm{Si}} = 14$ vs. $Z_{\mathrm{Ge}} = 32$.

The parameters used in the simulations (these include crystals' thickness, orientation with respect to the incident beam, curvature radii) have been chosen in accordance with the experiments [23, 25] performed at the Mainz Mikrotron (MAMI) facility. The thickness along the incident beam direction was $L = 15$ microns, which is comparable with the dechanneling length of 855 MeV electrons [17, 23, 40–43], thus increasing the efficiency of the orientational effects.

3. Beam-crystal alignment

In the experiments [23, 25], a uniform bending of $(11\bar{1})$ crystalline planes was achieved by means of a specially designed mechanical holder [34], which allowed one remotely alter the curvature radius thus making possible to investigate the deflection efficiency and the radiation intensity as functions of R. Bending of the planes occurs due to a secondary 'quasi-mosaic' (QM) deformation [44–46] that was the result of the primary deformation caused by the holder, see illustrative Fig. 1a. Prior to performing the beam experiment, the orientation of crystallographic directions was determined by means of a high-resolution X-ray diffraction [45], see Fig. 1b. This technique was also used to assess the uniformity of the crystal bending at different curvatures. Mounting crystals on a goniometer with three degrees of freedom provided high precision in the angular alignments between the samples and the incident beam [47].

Following the experimental setup, we have simulated passage of the electrons and calculated the emission spectra for the following two different beam–crystal alignments that can be illustrated by Fig. 1c:

(i) *Planar channeling alignment.* In this case, the beam velocity, being aligned at the entrance with the $(11\bar{1})$ plane, is directed at the angle θ with respect to the $\langle 112 \rangle$ axis. To avoid axial channelling, θ must to be chosen much larger than Lindhard's critical angle for the $\langle 112 \rangle$ axis (ca 0.4 and 0.6 mrad for Si and Ge
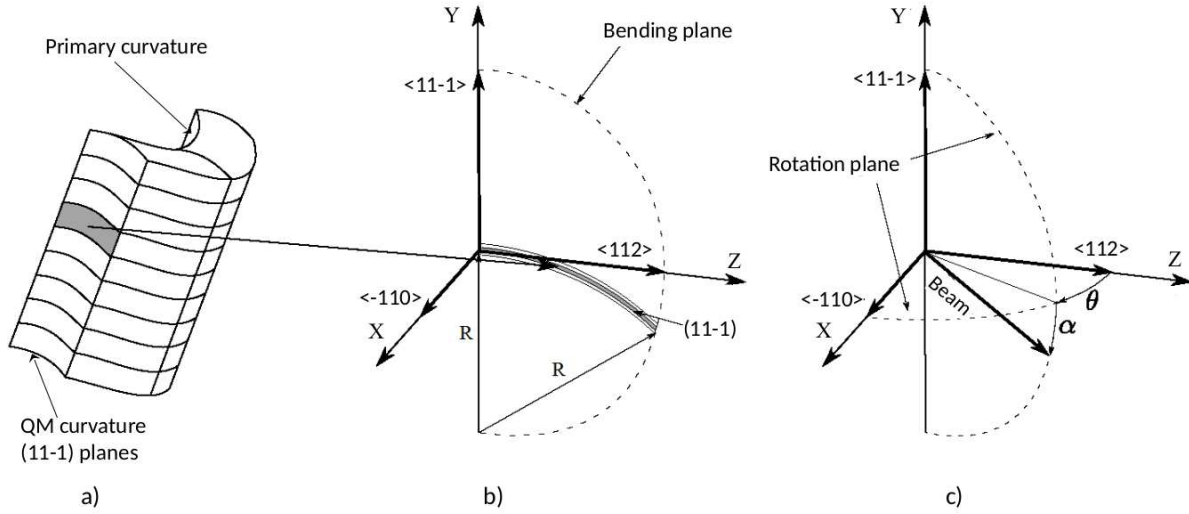
Figure 1. Crystal geometry and its orientation with respect to the incident beam that was used in the experimental setup and in the current simulations. *(a)* The $(11\bar{1})$ planes (the shaded area marks one of these) of the crystal experience the quasi-mosaic (QM) secondary bending as a result of primary curvature due to mechanical bending. *(b)* Crystallographic axes chosen for the Cartesian coordinate system. The (XZ) plane corresponds to the unbent $(11\bar{1})$ crystallographic plane. Shaded strip illustrates the QM bending; R denotes the radius of the QM curvature. *(c)* Angles used to characterize the incident electron beam velocity $\mathbf{v}_0$ relative to the crystal orientation: θ is the angle between $\mathbf{v}_0$ and the $\langle 112 \rangle$ axial direction, α – the angle between $\mathbf{v}_0$ and the unbent $(11\bar{1})$ plane.

crystals, respectively) but much smaller than 190 mrad that is the angle between the $\langle 112 \rangle$ and $\langle 123 \rangle$ axes [35]. In the current simulations the value $\theta = 95$ mrad was used. The second angle α, indicated in Fig. 1c, was set to zero.

(ii) *Volume reflection alignment* corresponds to the incident beam angle α within the range $\theta_{\mathrm{L}} \lesssim \alpha < L/R$ where $\theta_{\mathrm{L}} = (2U_0/\varepsilon)^{1/2}$ denotes Lindhard's critical angle for the planar channeling along the $(11\bar{1})$ planes. As a result, at the entrance most of the particles move in the over-barrier mode across the bent channels but later on in the bulk they can experience either volume capture or volume reflection [49,50].

Within the continuous potential approximation Lindhard's critical angle is given by $\theta_{\mathrm{L}} = (2U_0/\varepsilon)^{1/2}$ with U_0 standing for the depth of the continuous interplanar potential. Using the values $U_0 \approx 24$ eV for the Si$(11\bar{1})$ channel and $U_0 \approx 32$ eV for the Ge$(11\bar{1})$ channel, calculated within the Pacios approximation (see Fig. A3 in Section Appendix A), one obtains $\theta_{\mathrm{L}} \approx 0.24$ and 0.27 mrad for a 855 MeV electron channeling in the silicon and germanium crystals, respectively.

For each set (θ, α) considered in the simulations, to build the angular distribution of deflected electrons a large number, from $N \approx 4 \times 10^4$ up to 15×10^4, of trajectories have been simulated and analyzed. The computation of spectral distributions of the emitted radiation has been carried out using lower number of the trajectories, $N \gtrsim 10^4$. The analysis was performed for different values of the crystals' curvature.

To calculate the angular distributions, the trajectories have been simulated using the Moliére and the Pacios potentials for the electron–atom interaction. The analysis performed in Ref. [35] has shown that the Pacios approximation provides better agreement with the experiment for the spectrum of channeling radiation. Therefore, in the current paper the spectral dependencies have been obtained using this potential only.

Below in the paper, the statistical errors indicated for the simulated data are due to the finite number of the trajectories. The experimental data shown have been obtained by digitalizing the graphical data presented in Refs. [23,25]. Finite width of the lines used to draw experimentally measured angular distributions corresponds to the statistical errors of the data. The error bars for the experimental data on the emission spectra have not been indicated in the cited papers.

4. Case studies

4.1. Angular distribution of deflected electrons

Bending curvature of crystalline targets used in the experiment [23] was characterized in terms of the bending angle, $\theta_b = L/R$. For the crystals probed the quoted values of θ_b are $315, 550, 750, 1080$ μrad and $820, 1200, 1430$ μrad for the $L = 15$ μm thick Si and Ge crystals, respectively. Below in this section the curvature is specified in terms of the curvature radius, the corresponding values of which are as follows: $R = 47.6, 27.3, 20.0, 13.9$ mm for Si and $R = 18.3, 12.5, 10.5$ mm for Ge.

Distributions (in mrad^{-1}) shown below in this Section have been normalized to the unit area within the intervals of the deflection angle ϑ (in mrad) indicated in Ref. [23].

The deflection angle stands for the projection of the angle between initial $\mathbf{v}_0$ and final $\mathbf{v}$ velocities of the projectile electron on the plane that contains $\mathbf{v}_0$ and the $\langle 11\bar{1} \rangle$ axis.

4.1.1. Channeling alignment   Figure 2 presents angular distributions of electrons after passing through bent silicon (top graph, $R = 47.6$ mm, $\theta_b = 0.315$ mrad) and germanium (bottom graph, $R = 18.3$ mm, $\theta_b = 0.820$ mrad) crystals. The incident particle's velocity $\mathbf{v}_0$ is directed along the $(11\bar{1})$ crystallographic plane.

Two maxima are distinguishable in the curves presented. The left one, located in the vicinity of $\vartheta = 0$, is mainly due to the electrons that experience the over-barrier motion at the crystal entrance. The right maximum, centered at $\vartheta = \theta_b$, corresponds to the projectiles that move in the channeling mode at the crystal exit. Its width equals to Lindhard's critical angle θ_L.

On average, the scattering angle in electron collisions with heavier germanium atom is larger than with a silicon atom. This relation also holds for the multiple scattering angles in germanium and silicon media. As a result, (i) the over-barrier peak in the distribution for the silicon target is higher and narrower than for the germanium target,
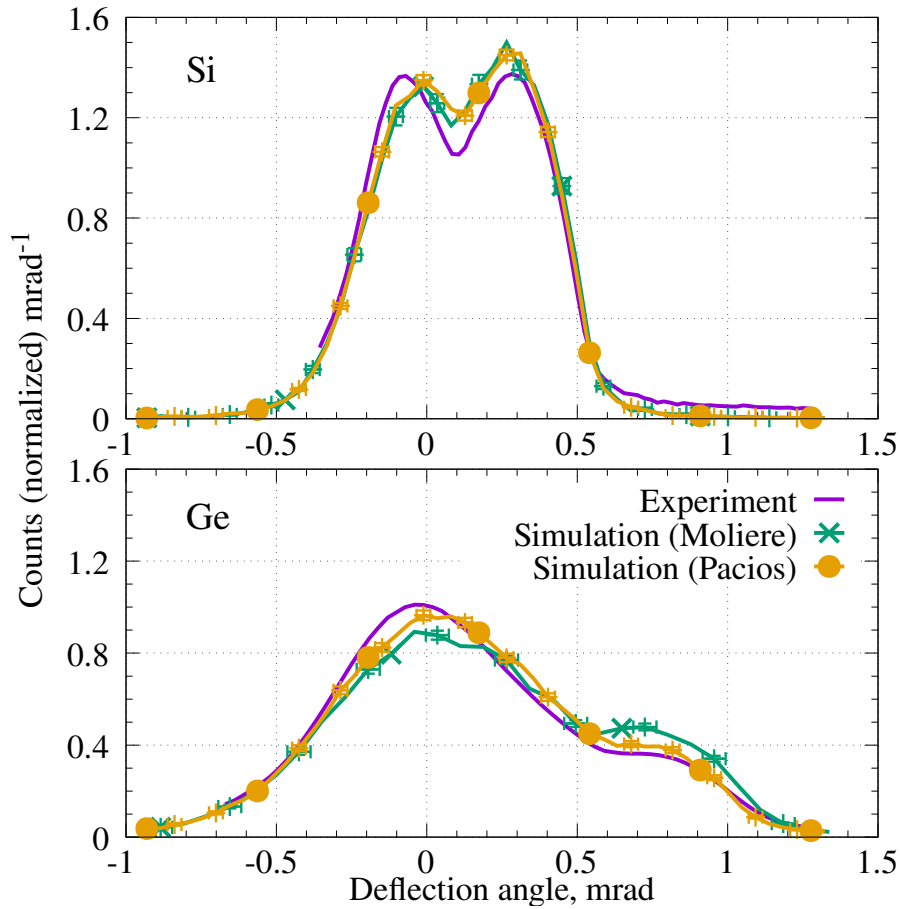
Figure 2. Simulated versus experimentally measured (see Ref. [23]) angular distributions of deflected electrons in the case of the channeling alignment of the incident beam with the $(11\bar{1})$ plane. The incident angles are $\theta = 95$ mrad, $\alpha = 0$, see Fig. 1. The simulations has been carried out with both the Moliére and Pacios atomic potentials. The curvature radius R of the plane equals to 47.6 mm ($\theta_b = 0.315$ mrad) for the silicon crystal target (top) and to 18.3 mm ($\theta_b = 0.820$ mrad) for the germanium crystal (bottom).

(ii) the dechanneling rate in Ge crystal is notably larger than in Si, so that the channeling peak in the bottom graph in Fig. 2 is much less intensive than in the top graph. Analysis of the trajectories simulated in these case studies has shown that approximately 30 % of the electrons incident on the Si target pass through the crystal moving in the channeling mode whereas for the Ge target this number is much lower, 5 %.

For the silicon target, a discrepancy between the distributions calculated using the Moliére and Pacios atomic potentials are within the statistical uncertainties whereas for the germanium crystal the difference between the distributions is clearly seen in the vicinities of both maxima. For the heavier crystal, the Pacios approximation, being more accurate in description of the atomic potential (see Appendix Appendix A), results in a better agreement of the simulated angular distribution with the experimentally measured one.
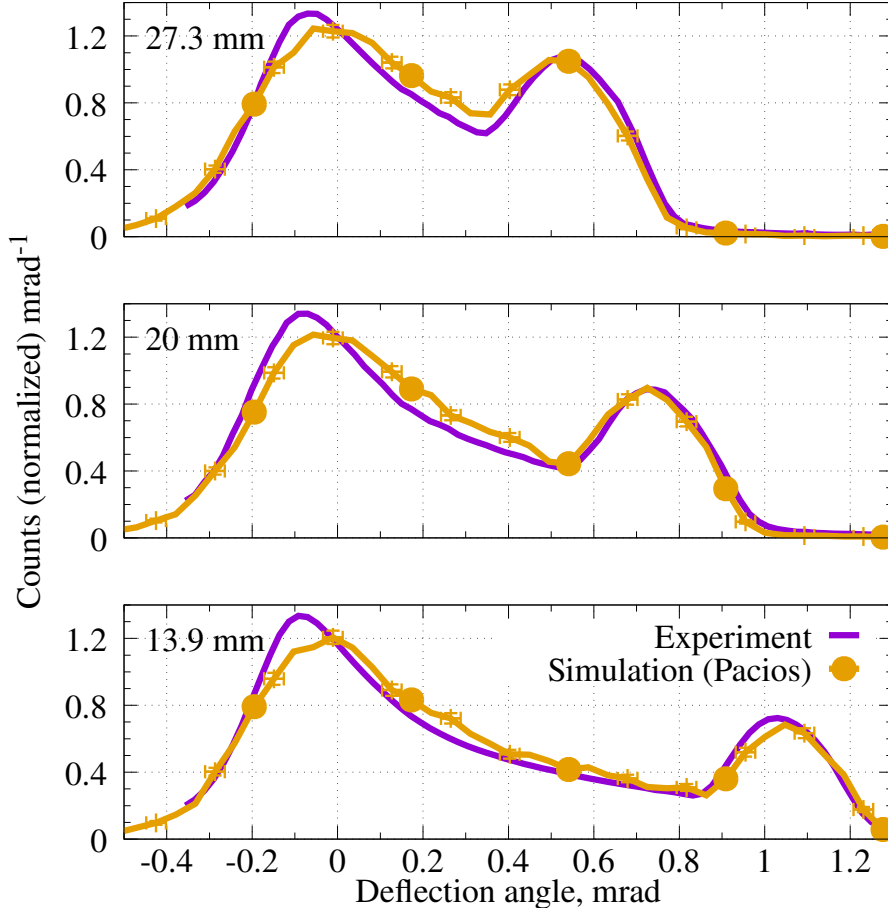
Figure 3. Angular distribution of deflected electrons after interaction with bent Si crystal as a function of the curvature radius R of the $(11\bar{1})$ plane: $R = 27.3$ mm (top), 20 mm (middle) and 13.9 mm (bottom). The incident beam geometry corresponds to the planar channeling alignment with $\theta = 95$ mrad and $\alpha = 0$. The experimental data are from Refs. [23,35]. The results of the simulations shown correspond to the Pacios atomic potential.

Evolution of the angular distribution with decrease in the curvature radius (increase in the bending angle) of the silicon crystal is demonstrated by Fig. 3. The values of R indicated in the top, middle and bottom graphs correspond to $\theta_{\rm b} = 0.55, 0.75, 1.08$ mrad. It is seen that the position of the channeling peak in the simulated distribution follows the quoted $\theta_{\rm b}$ values and its position, height and width agree well with the experimental data. In all simulated distributions the position and height of the maximum due to the over-barrier particles at the entrance are the same within the statistical errors. There are systematic deviations from the experiment. First, the simulation underestimates (by ca 10 %) the peak values of the maxima. Second, the experimentally measured distributions are peaked at $\vartheta \approx -0.08$ mrad whereas the maxima in the simulated distributions are less shifted to the domain of negative scattering values. Finally, the simulation produces higher values in the region between both peaks which corresponds to the higher dechanneling rate.
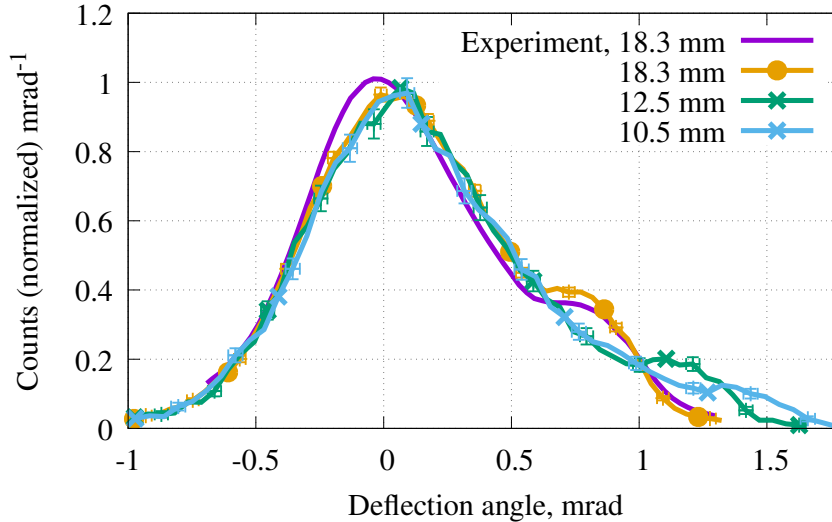
Figure 4. Angular distribution of deflected electrons after interaction with bent Ge crystal as a function of the curvature radius R of the $(11\bar{1})$ plane as indicated in the legend. The incident beam geometry corresponds to the planar channeling alignment with $\theta = 95$ mrad and $\alpha = 0$. The experimental data for $R = 18.3$ mm are from Ref. [23]. The results of the simulations shown correspond to the Pacios atomic potential.

Angular distribution of the electrons deflected by germanium crystals bent with different curvature radii are shown in Fig. 4. In Ref. [23] the experimental data are presented only for $R = 18.3$ mm ($\theta_{\mathrm{b}} = 0.82$ mrad). As in the case of the silicon crystal, the position of the channeling maximum is shifted towards higher deflection angles as the bending curvature $1/R$ increases. Its peak value becomes less intensive due to higher dechanneling rates for larger curvatures.

For all curvature radii considered the distributions of the over-barrier electrons at the entrance obtained in the simulations are centered at $\vartheta \approx 0$. The experimentally measured distribution exhibits some shift towards negative values of the deflection angle.

In Ref. [23] the fitting procedure is described which has been used to extract the dechanneling length L_{d} and channeling efficiency η from the angular distributions. The channeling efficiency has been defined as the integral value of the gaussian fit of the channeling peak carried out over the interval $\pm$ three standard deviations from the peak's position.

Within the relativistic molecular dynamics framework utilized in this paper, these quantities can be calculated directly by means of statistical analysis of the trajectories (see Ref. [17] for more details). To determine the average interval within which a particle moves in the channeling mode starting at the crystal entrance one can analyse the trajectories of the accepted particles. An accepted projectile, stays in the channeling mode of motion over some interval until an event of the dechanneling (if it happens within the crystal thickness considered). Hence, the dechanneling effect for the accepted particles can be characterized in terms of the penetration length L_{p} [36] defined as

the arithmetic mean of the initial channeling segments L_{ch0} calculated with respect to all accepted trajectories: $L_{\mathrm{p}} = N_{\mathrm{acc}}^{-1} \sum_{j=1}^{N_{\mathrm{acc}}} L_{ch0}^{(j)}$. The channeling efficiency is defined through the ratio $\eta = N_{\mathrm{ch}}/N$ where N is the number of the incident electrons and N_{ch} stands for the number of electrons that leave the crystal in the channeling mode (this number accounts for the projectiles that channel through the whole crystal as well as for those that were captured in the channeling mode somewhere in the bulk and channel till the crystal exit).

Table 1. Curvature radius, R, bending angle, θ_{b}, penetration length L_{p} and channeling efficiency η for silicon and germanium crystals. Three last columns present experimentally measured dechanneling length, $L_{\mathrm{d,exp}}$, and channeling efficiency η_{exp} and the simulated value of channeling efficiency [23].

	R	θ_{b}	L_{p}	η	$L_{\mathrm{,exp}}$	η_{exp}	η_{sim}
	(mm)	(mrad)	(μm)		(μm)		
Si	27.3	0.55	15.7±0.3	0.30±0.02	17.7±3.0	0.248±0.016	0.3000
	20.0	0.75	14.8±0.4	0.24±0.02	14.0±2.2	0.206±0.013	0.2519
	13.9	1.08	13.1±0.3	0.18±0.01	10.1±1.0	0.165±0.010	0.1907
Ge	18.3	0.82	7.3±0.2	0.110±0.010	9±5	0.084±0.017	0.0909
	12.5	1.20	6.8±0.1	0.058±0.011	7.3±1.2	0.036±0.007	0.0468
	10.5	1.43	6.4±0.2	0.037±0.011	5.9±1.5	0.019±0.004	0.0320

Table 1 summarizes the values of L_{p} and η that have been calculated for silicon and germanium crystals with the bending parameters as indicated. Also presented are the data from Ref. [23] (see tables 1-3 there): experimentally measured dechanneling lengths and channeling efficiency as well as the latter quantity, notated as η_{sim}, obtained by means of the CRYSTAL code [48] (we quote the η_{sim} values without the statistical uncertainties which are within the range $(2 - 4) \times 10^{-4}$).

It is seen that with account for the statistical errors our results for L_{p} fully correlate with the experimental data for L_{d} (as well as with the results obtained with the CRYSTAL that is not shown here but can be found in table 3 in Ref. [23]).

For the germanium crystals the values of channeling efficiency obtained in the current simulations are systematically higher than measured experimentally. We note, however, that similar tendency is seen in η_{sim}, see the last column in Table 1.

4.1.2. Volume reflection alignment In second case study, the geometry of which is illustrated in 1c, the beam was incident at the angle $\alpha = 0.45$ mrad with respect to the $(11\bar{1})$ plane, which is larger than Lindhard's critical angles in Si and Ge crystals. Hence, at the crystal entrance the electrons are not accepted into the channeling mode of motion. In this case, due to the bending of crystalline planes that results in the asymmetry of the interplanar potential, a particle can be captured into the channeling mode somewhere in the crystal volume (volume capture) or be reflected from the interplanar potential barrier (volume reflection). The volume capture leads to

the appearance of the channeling peak in the angular distribution whereas the volume reflection shifts the over-barrier peak to the domain of negative deflection angles.
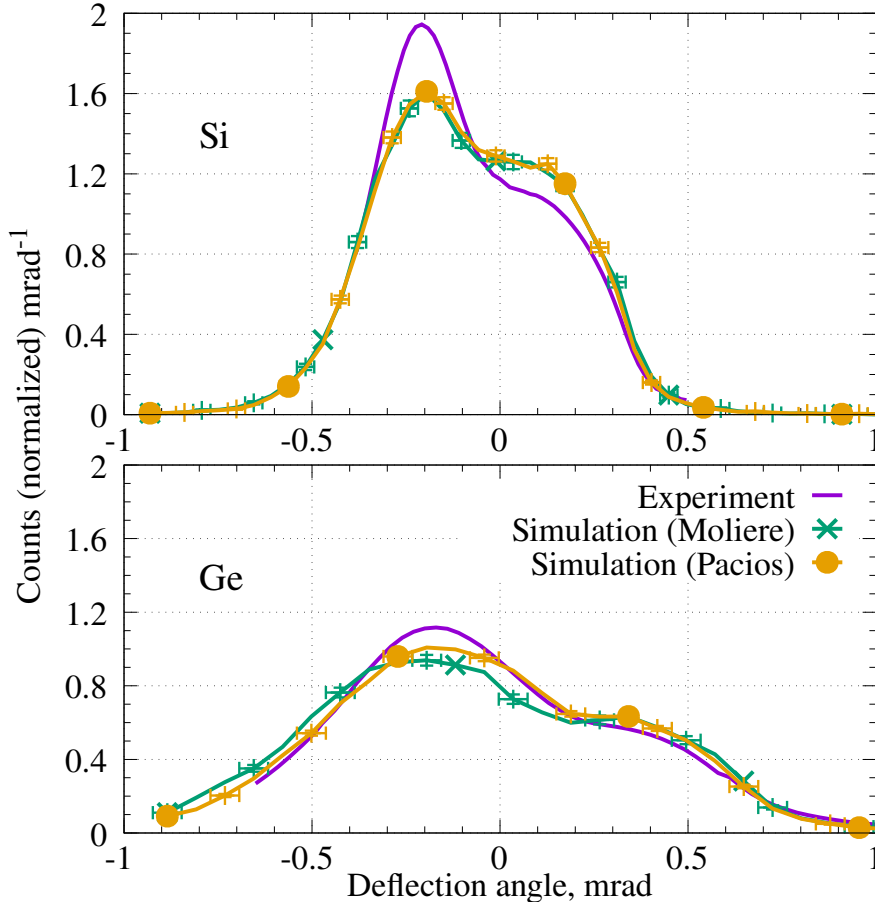

Figure 5. Angular distribution of deflected electrons after interaction with Si(11$\bar{1}$) crystal (top) bent with $R = 47.6$ mm ($\theta_b = 0.315$ mrad) and Ge(11$\bar{1}$) crystal (bottom) bent with $R = 18.3$ mm ($\theta_b = 0.820$ mrad). The experimentally measured [23] and the simulated distributions correspond to the volume reflection alignment with $\alpha = 0.45$ mrad and $\theta = 95$ mrad, see Fig. 1c.

Figure 5 compares the results of the simulations carried out for bent silicon ($R = 47.6$ mm, $\theta_b = 0.315$ mrad) and germanium ($R = 18.3$ mm, $\theta_b = 0.820$ mrad) crystals with the experimental data from Ref. [23].

For comparison, the simulations have been performed utilizing each one of the atomic potentials. As in the case of the channeling geometry, Fig. 2, both atomic potentials produce similar (within the statistical error) angular distributions for the silicon target whereas for the germanium crystal the difference between them is clearly seen.

The simulations follow the experiment in reproducing the changes in the angular distributions as compared to the channeling alignment. To be noted is the shift, by approximately -0.2 mrad for both crystals, of the over-barrier peak caused by the volume-deflected electrons. The contribution of these electrons explains the increase

in the peaks' values in comparison with the over-barrier maxima in Fig. 2.

The channeling peaks, however, are modified differently for the silicon and germanium targets both in terms of the shift and the peak value. Let us first consider the Ge crystal, Fig. 5 bottom. The incident angle $\alpha = 0.45$ mrad is smaller than the bending angle $\theta_b = 0.820$ mrad, therefore, geometrically, the line drawn along the beam direction $\mathbf{v}_0$ becomes tangent to the bent plane at the distance $l = L(\theta_b - \alpha)/\theta_b \approx 7$ μm from the crystal exit. Since l is ca 2 times less than the crystal thickness, a particle that experiences volume capture at this distance has much higher probability to exit in the channeling mode than the same particle accepted at the entrance in the channeling geometry. These qualitative arguments explain the increase in the channeling peak intensity for Ge in Fig. 5 in comparison to that in Fig. 2, as well as the shift of the position: instead of 0.820 mrad the maximum is at ca $\theta_b - \alpha = 0.37$ mrad. For the silicon crystal, Fig. 5 top, the geometrical approach has to be modified since in this case $\alpha > \theta_b = 0.315$ mrad so that the line $\mathbf{v}_0$ does not touch the curved channel. Assuming that a particle can be accepted into the channeling mode if its local incident angle with respect to the plane is less than Lindhard's critical, one estimates that some fraction of electrons can experience volume capture at the distances $l = L(\theta_L + \theta_b - \alpha)/\theta_b \approx 5$ μm. The probability for an electron to channel over such distance is high enough, however, the number of volume capture events is smaller than the number of the accepted particles in the case of the channeling alignment. As a result, the channeling peak in Fig. 5 top is lower than that in Fig. 2 top.

Apart from the aforementioned similarities, there are differences in the distributions' maxima values measured experimentally and obtained via the simulations. The differences are more pronounced for the Si target: the experimental over-barrier peak is ca 20% higher whereas the channeling peak is lower by approximately the same amount. For the Ge crystal the simulation-to-experiment agreement is better if one considers the curve corresponding to the Pacios potential: the maxima differ by 10%.

4.2. Radiation spectra

Characterization of the radiation emitted by the beam passing though a target can be done in terms of spectral distribution of the radiant energy, $E\mathrm{N}/\mathrm{E}$. Here N stands for the number of photons emitted within the energy interval $[E, E + \mathrm{E}]$. To compute the spectral distribution, the trajectories simulated with the use of the Pacios potential have been utilized further following the formalism and algorithm described in detail in Ref. [36]. To obtain $E\mathrm{N}/\mathrm{E}$ per particle, first the spectral-angular distribution was calculated for each trajectory, then it was integrated over the cone $\theta_0 = 4.65$ mrad along the incident beam, and the results were averaged over all trajectories. The quoted value of θ_0 is approximately eight times larger than the natural emission cone γ^{-1} of a 855 MeV electron and is also much larger than the bending angles $\theta_b = L/R$ (see below). Therefore, the calculated spectra accounted practically for all radiation emitted by the projectile particles.

The spectral distributions have been calculated for the planar channeling and volume reflection alignments. Both cases refer to the motion in an oriented crystalline target where a projectile experiences collective action of the electrostatic fields of the atoms. This leads to the increase in the radiant energy as compared to that emitted in the corresponding amorphous medium via the incoherent bremsstrahlung process. To quantify the latter process, the trajectories of 855 MeV electrons passing through 15 microns thick amorphous silicon and germanium targets have been simulated followed by the calculation of the spectral distributions as described above. For the sake of reference, the values of $E\dot{N}/\dot{E}$ calculated for the amorphous media are presented below:

$$E\frac{\dot{N}}{\dot{E}}\bigg|_{Si,am} = (0.21 \pm 0.02) \times 10^{-3}, \qquad E\frac{\dot{N}}{\dot{E}}\bigg|_{Ge,am} = (0.85 \pm 0.05) \times 10^{-3}. \qquad (3)$$

These values, that characterize the incoherent bremsstrahlung background within the photon energy range $E = 1 - 10$ MeV, are consistent with the data measured experimentally, see figure 2 in Ref. [25]. The intensity of radiation in the amorphous germanium environment is approximately four times higher than in the silicon one. This factor correlates with the ratio of atomic numbers squared.

In the cited paper the curvature of crystals was quantified in terms of the bending angle θ_b equal to $550, 750, 1080$ μrad for the silicon crystal and to $820, 1200, 1430$ μrad for the germanium crystal. For the thickness $L = 15$ μm these values produce the curvature radii (in mm) equal to $27.3, 20.0, 13.9$ and $18.3, 12.5, 10.5$, correspondingly.

4.2.1. Channeling alignment   For the channeling alignment, comparison of spectral distributions measured experimentally [25] and calculated within the current simulations is presented by Fig. 6 (silicon) and Fig. 7 (germanium). One can note an overall good agreement between the experiment and the theory.

A common feature, seen for both crystals and all curvature radii, is an increase in the radiation intensity in the oriented targets in comparison to its values in the amorphous media, Eq. (3). For Si crystal bent with $R = 27.3$ mm the enhancement factor is about eight at the photon energy $E \approx 2$ MeV . For the Ge crystal with $R = 18.3$ mm it stays equal to approximately three over a wide range of the photon energies.

The enhancement is mainly due to the emission by the particles that move in the channeling mode of motion. As the bending curvature $1/R$ increases, the average length of the channeling segment, $\langle L_{ch} \rangle$, decreases resulting in the decrease in the radiant energy which is proportional to $\langle L_{ch} \rangle$. For silicon crystals with $R = 27.3$ and 13.9 mm, statistical analysis of the lengths of all channeling segments in all trajectories simulated has led to $\langle L_{ch} \rangle = 7.5 \pm 0.1$ and 5.8 ± 0.1 μm, respectively. The ratio of the central values, $7.5/5.8 \approx 1.3$, nicely correlates with the height of the peak at $E \approx 2$ MeV in the top ($E\dot{N}/\dot{E} \approx 1.6 \times 10^{-3}$) compared to that in the bottom ($E\dot{N}/\dot{E} \approx 1.2 \times 10^{-3}$) graphs in Fig. 6. Similar calculations performed for the germanium targets resulted in $\langle L_{ch} \rangle = 4.8 \pm 0.1$ and 3.5 ± 0.1 μm for $R = 18.3$ and 10.5 mm, which also corresponds to the ratio of the intensities in the top and bottom graphs in Fig. 7.
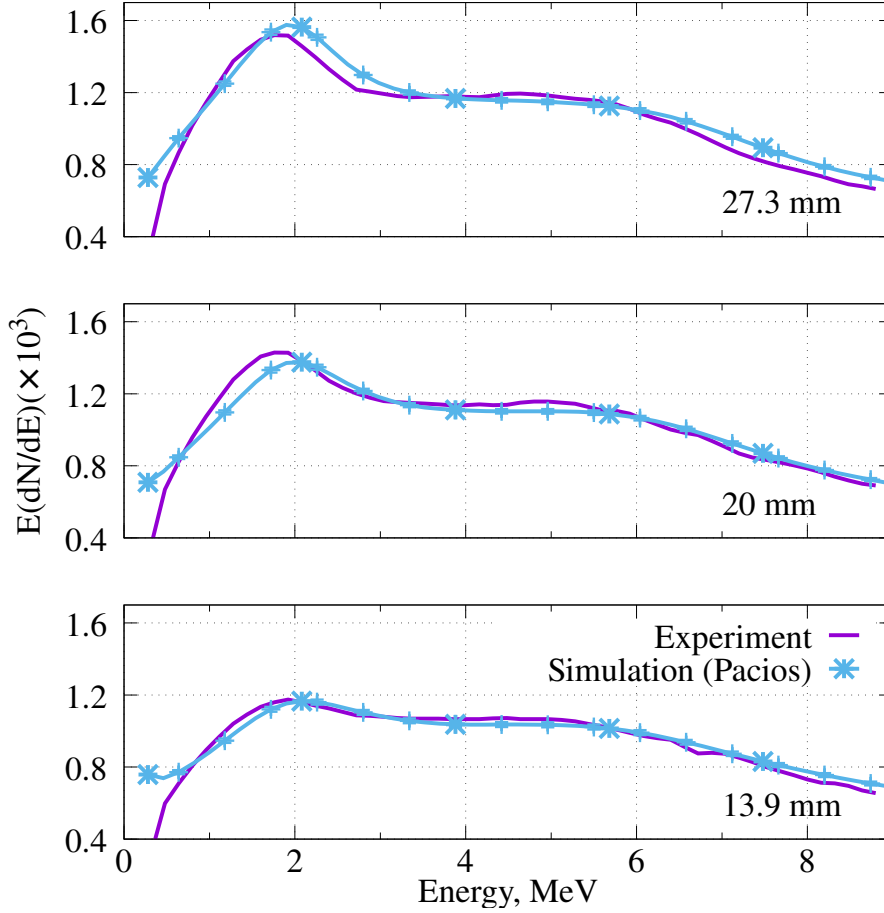
Figure 6. Spectral distribution of radiation emitted by 855 MeV electrons passing through Si(11$\bar{1}$) crystal bent with the curvature radius 27.3 mm (top), 20 mm (middle) and 13.9 mm (bottom). The incident beam geometry corresponds to the planar channeling alignment with $\theta = 95$ mrad and $\alpha = 0$. Experimental data are taken from [25]. Note that the values of EN/E shown are multiplied by the factor 10^3.

As in the case of amorphous environment, the intensity in oriented germanium crystal is higher that in the silicon crystal, although the excess is not as large as for the amorphous targets, see Eq. (3). Partly, this change is due to the excess of $\langle L_{ch}\rangle_{Si}$ over $\langle L_{ch}\rangle_{Ge}$.

A feature, which distinguishes the spectra in Si and Ge, refers to the peak of channeling radiation seen in the Si spectra at $E \approx 2$ MeV but not pronounced for Ge. An initial intuitive explanation could be as follows. To a great extent, the peaks are due to the radiation emitted by electrons that move in the channeling mode through the whole crystal. For the silicon crystal the fraction of such particles with respect to the number of incident particles is quite large, being approximately equal to 25%, 20%, 16% for the R values indicated in Fig. 6 from top to bottom. For the germanium target the fraction is nearly an order of magnitude smaller, equal to 3.6%, 2.5% and 1.9% with reference to Fig. 7. In this case, main contribution to the spectrum comes from the over-barrier projectiles, which radiate in a broader energy range and, thus, level the
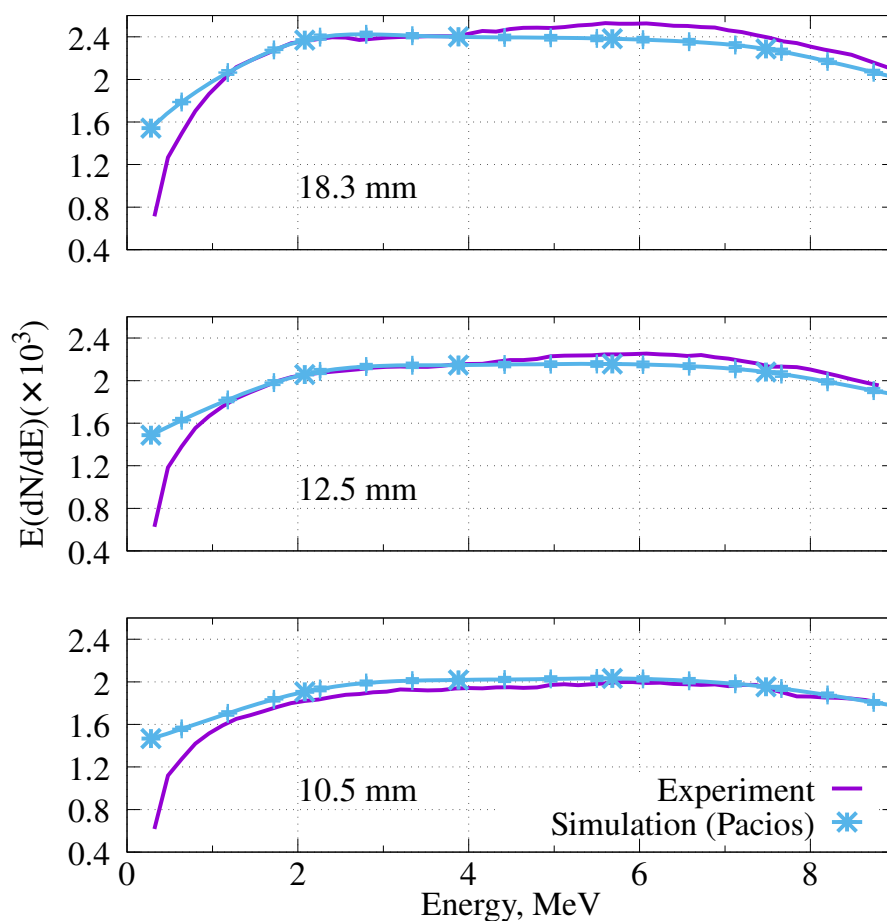
Figure 7. Same as in Fig. 6 but for Ge(11$\bar{1}$) crystal. The curvature radii are indicated in each graph.
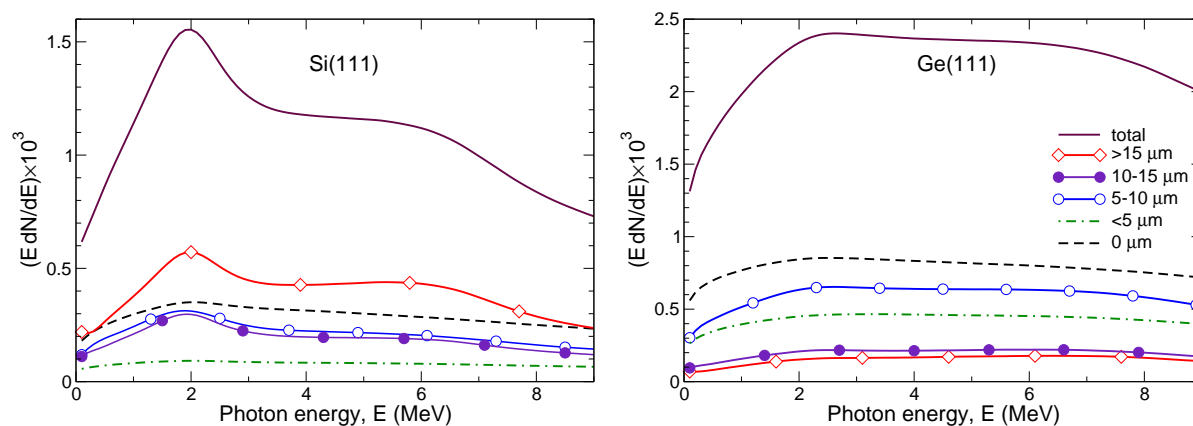
spectrum's shape.

Figure 8. Spectral distribution of radiation in Si ($R = 27.3$ mm, left graph) and Ge (18.3 mm, right graph) bent crystals with explicit contributions from different group of particles as indicated in the common legend in the right graph. See explanations in the text. The incident beam geometry corresponds to the planar channeling alignment.

To check this hypothesis, one can analyse the contributions of different groups of particles to the total spectrum. The result of this analysis is presented in Fig. 8 for crystals bent with the largest curvature radii: Si with $R = 27.3$ mm (left) an Ge with $R = 18.3$ mm (right). In both graphs solid curve shows the total spectrum (per particle); solid line + diamonds stands for the contribution from the electrons that move in the channeling mode through the whole crystal; solid line + closed circles, solid line + open circles and dash-dotted line denote the contribution from the electrons with the initial channeling segment L_{ch0} (in microns) lying within the interval: $10 \leq L_{ch0} < 15$, $5 \leq L_{ch0} < 10$, and $0 \leq L_{ch0} < 5$, respectively. The contribution from the trajectories that have no initial channeling segments (but which can have those in the bulk) is shown with dashed line. For Si, the main channeling peak is indeed due to the particles that channel through the whole crystal (30% of the peak intensity). The emission spectra of the particles that channel over considerable part of the crystal (the curves with the circles of both types) are also enhanced at $E \approx 2$ MeV. The emission of other particles provide a smooth background. In contrast, with respect to the shape of the spectrum, all groups of particles passing through the germanium crystal, including those which move in the channeling mode radiate similarly: a smooth curve with nearly constant value within the interval $E = 2 - 8$ MeV.
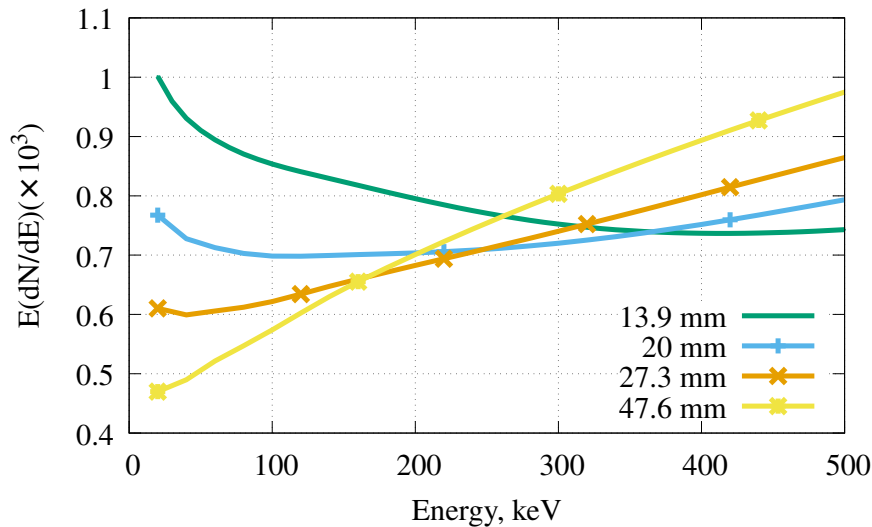

Figure 9.   Low-energy part of the radiation spectra by 855 MeV electrons in bent Si crystal calculated for different curvature radii R as indicated. The increase in the spectra as the photon energy decreases, seen for all radii but $R = 47.6$ mm, is due to the synchrotron radiation. The incident beam geometry corresponds to the planar channeling alignment with $\theta = 95$ mrad and $\alpha = 0$.

An additional feature that appears in the emission spectrum in a bent crystal as compared to a linear crystal is due to a circular motion of the channeling particles. This motion gives rise to the synchrotron-type radiation, which contributes to the low-energy part of the spectrum. This feature was predicted theoretically long ago [13, 14] and has also been analysed quantitatively by means of all-atom relativistic molecular dynamics

simulations [41, 42, 51]. The characteristic energy E_c beyond which the synchrotron radiation intensity rapidly falls off [52] can be written as follows: $E_c\,[\text{MeV}] = 2.21\varepsilon^3/R$ with ε in GeV and R in millimeters. For a 855 MeV projectile and for $R \gtrsim 10$ mm one estimates $E_c \lesssim 10^{-1}$ MeV. Figure 9 presents a low-energy part, $E = 20 - 500$ keV, of spectral distribution of radiation emitted in the silicon crystals with different curvature radii. As mentioned above, the spectral distributions correspond to the emission cone that accounts practically for all radiation emitted by the projectiles. This results, in particular, in the increase of the synchrotron-like radiation intensity with the curvature. Figure 9 shows that in the in the energy range $E_c \leq 250$ keV the most intensive radiation is formed in the crystal with the smallest curvature radius, $R = 13.9$ mm.

The radiation emission within this energy range has not been measured in Ref. [25]. However, the phenomenon of the synchrotron-like radiation emitted by ultra-relativistic projectiles in different oriented bent crystals deserves experimental investigation especially in view of the ongoing efforts of the research and technological communities towards design and practical realization of novel gamma-ray crystal-based light sources [9, 53].

4.2.2. Volume reflection alignment   Spectral distributions of radiation emitted by the electron beam incident on the crystals at the volume reflection alignment are presented in Fig. 10 and 11. The results of simulations follow the experimentally measured dependencies and reproduce the modifications in the spectra observed in Ref. [25].

For both crystals the radiation intensity in the volume reflection geometry is smaller than under the channeling condition, Figs. 6 and 7, although the reduction is not dramatic so that in a broad range of photon energies the intensities are noticeably higher that in the amorphous targets. The decrease in the $E(N/E)$ values is more pronounced for larger curvature radius since the change in the geometry affects the channeling efficiency which is higher in the crystals bent with less curvature. For the germanium crystal the decrease is quite moderate, varying from approximately 20% for $R = 18.3$ mm down to 10% for $R = 10.5$ mm. For the silicon crystal the decrease is larger. Comparing the peak values of the channeling radiation at $E \approx 2$ MeV one observes the drop in the intensity by, approximately, 40% and 25% for the largest and the smallest curvature radius, respectively.

5. Conclusions

By means of relativistic all-atom molecular dynamics implemented in the MBN EXPLORER software package, the passage of ultra-relativistic electrons through 15 μm thick silicon and germanium bent crystals has been simulated. The bending curvatures and the alignments of the 855 MeV electron beam with respect to the crystallographic directions utilized in the simulations correspond to those used in the experiments [23, 25, 35]. carried out at the MAMI facility. The alignments considered include (i) the channelling alignment, when the beam is aligned with the tangent to the $(11\bar{1})$
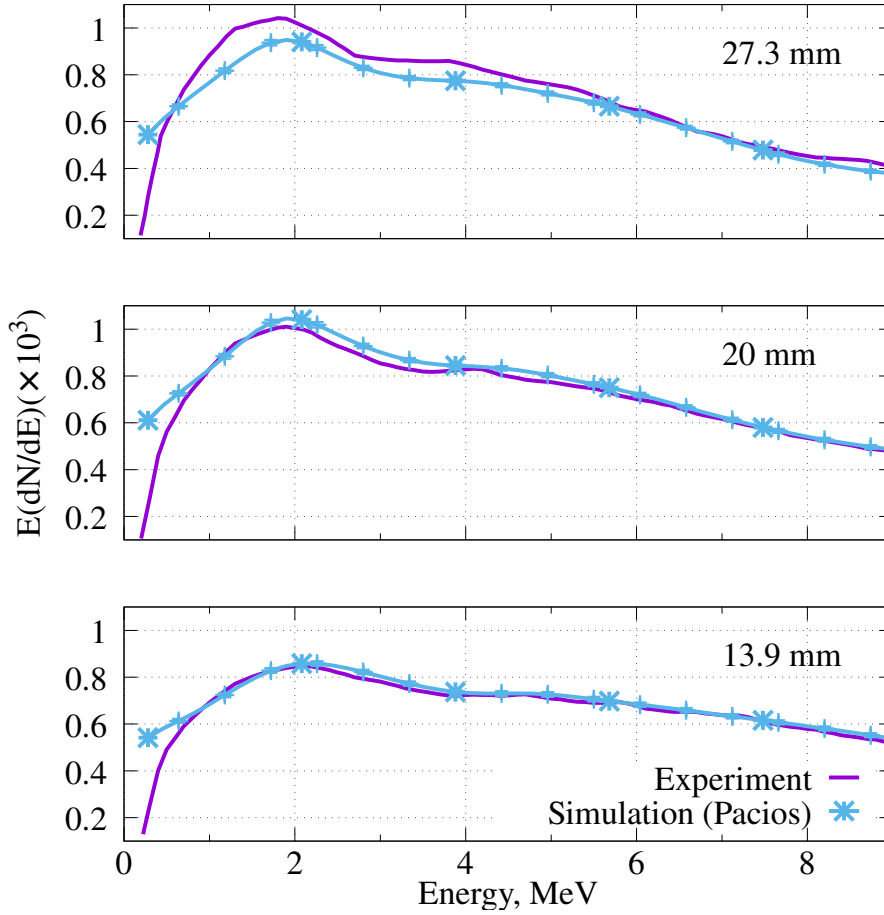
Figure 10. Spectral distribution of radiation emitted by 855 MeV electrons passing through Si(11$\bar{1}$) crystal bent with the curvature radius 27.3 mm (top), 20 mm (middle) and 13.9 mm (bottom). The incident beam geometry corresponds to the volume reflection alignment with $\theta = 95$ mrad and $\alpha = 0.385$, 0.375 and 0.540 mrad in the top, middle and bottom graphs, respectively. Experimental data are from [25].

planar direction at the entrance, and (ii) the volume reflection regime. For each case study considered, a sufficiently large number of statistically independent trajectories has been generated. Subsequent analysis of the trajectories resulted in the calculation of the angular distribution of the electrons deflected by a crystalline target, and the spectral distribution of radiation emitted by the beam particles. The simulations have been performed using two approximations for the electron–atom interaction, due to Moliére and to Pacios. We have established that both approximations provide similar results for the silicon crystal but in the case of the heavier germanium crystal the Pacios approximation is more adequate.

Our results exhibit a high degree of agreement with the experimental data especially in terms of the profiles of the angular and spectral distributions as well as in the positions of the maxima that are due to the channeling motion. In case (i) main discrepancies have been revealed in the angular distribution of electrons in the vicinity of the over-barrier peak. In case (ii) there are differences in the angular distributions' maxima values. The
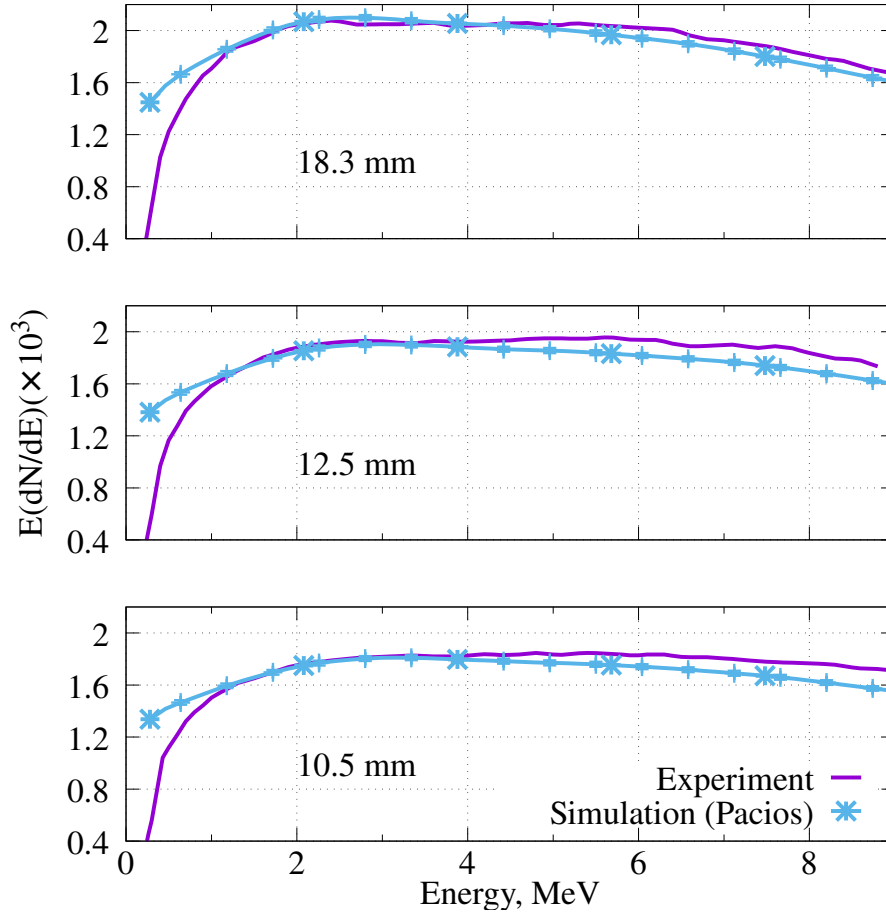
Figure 11. Same as in Fig. 10 but for bent germanium crystals. The curvature radii are indicated in each graph. The simulations were performed for the volume reflection alignment with $\alpha = 0.410$ (top), 0.600 (middle) and 0.715 (bottom) mrad.

differences are more pronounced for the silicon crystal: the experimental over-barrier maximum is 20% higher than the result of simulation whereas the channeling maximum is lower by approximately the same amount. For the Ge crystal the agreement is better: the maxima differ by 10%.

Two features, which were present in the experimental setup but have not been accounted for in the present work, could be the cause of the discrepancies. First, in the simulations we have disregarded the beam size of 105 μm and angular divergence of 21 μrad divergence in the plane of the crystal bending as quoted in Refs. [23,25]. Secondly, when simulating the structure of quasi-mosaically bent crystal, the secondary anticlastic curvature has not been taken into account. However, it has been demonstrated recently [54] that the accurate quantitative description of experimental results on the beam deflection by such crystals can only be achieved if one accounts for beam size and divergence as well as deduces the entrance coordinate of the beam center in the plane of the anticlastic bending. In the cited paper the effect of the secondary anticlastic curvature on the angular distribution of deflected electrons has been analysed in connection with the experiment at the SLAC facility [6]. We are planning to carry

out similar analysis for the experiments with the electron beam at MAMI.

Acknowledgements

Appendix A. Atomic and interplanar potentials

For the sake of reference, we present numerical data for atomic and (111) interplanar electron potentials calculated using the approximations due to Moliére [37], Doyle and Turner [39], and Pacios [38]. Explicit formulae used in the calculations can be found in Ref. [17]. For brevity, below the abbreviations M, D-T and P are used when referring to the approximations.

Atomic potentials U_a of Si and Ge atoms are compared in Figure A1. The curves shown present the dependencies of the scaled potential, $rU_a(r)/Z$, on the radial distance measured in the Thomas-Fermi radius a_{TF}, which is equal to 0.194 and 0.148 Å for Si and Ge atoms, respectively. In the domain $r \gtrsim 2a_{TF}$, the P and D-T curves practically coincide lying below the M curve. This discrepancy is larger for the higher-Z atom. At small distances, the D-T parametrization is incorrect whereas both M and P schemes provide the same result that lead to the correct limit $rU_a(r)/Z \to 1$ as $r \to 0$.

Within the continuous potential framework [1] the potential of an atomic plane in a crystal is obtained by summing up potentials U_{at} of the atoms in the plane assuming that they are distributed uniformly within the plane. This procedure also includes averaging of the atomic positions due to thermal vibrations. The inter-planar potential U_{pl} is calculated as a sum of the potentials of individual planes.

Silicon and germanium have the diamond cubic crystal structure with lattice constants a equal to 5.43 and 5.66 Å, respectively. Distance between the (111) planes changes periodically from the large distance equal to $3a/4$ to the small one $a/4$, see illustrative Fig. A2. For a negatively charged projectile (an electron, in particular) the (111) channel includes two planes separated by $a/4$. As a result, the continuous inter-planar potential as a function of the distance ρ from the channel's center (dot-dashed line in the figure) has two symmetric minima located at $\rho = \pm a/4$.

Two graphs in Fig. A3 compare the M, P and D–T electron's inter-planar potentials $U_{pl}(\rho)$ in silicon and germanium crystals. The uniform distribution of the atoms within a plane removes the aforementioned incorrect feature of the Doyle-Turner *atomic* potential. It is seen that in the planar case the P and D-T approximations converge to practically the same results while the M approximation produces higher values (10 % and 25 % for silicon and germanium, respectively) for the depth of the potential well.
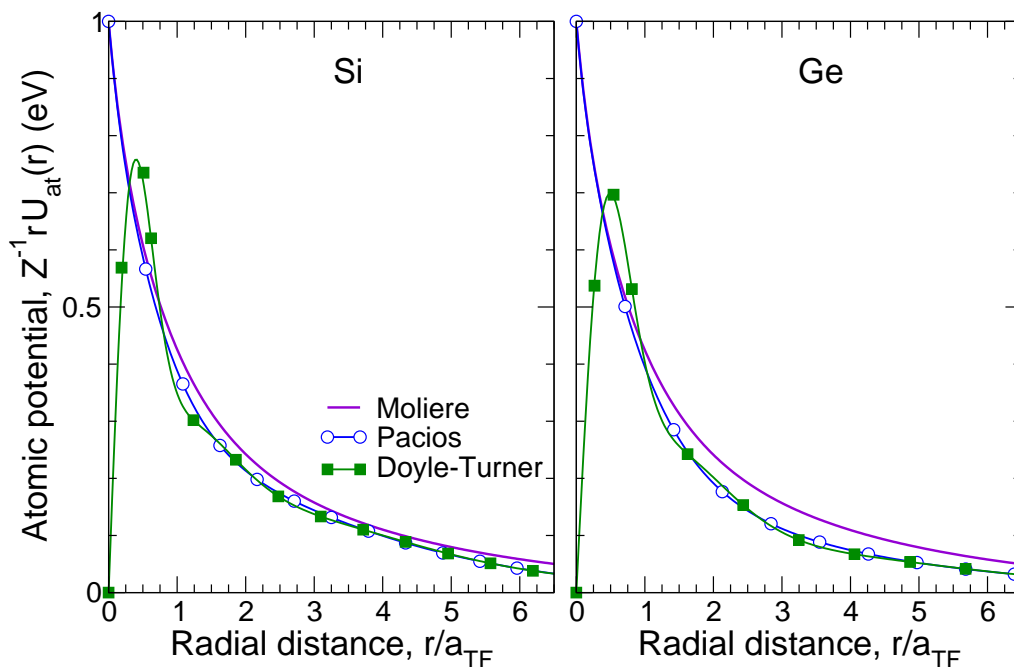
Figure A1. Scaled atomic potentials $rU_\mathrm{a}(r)/Z$ versus scaled radial distance r/a_TF calculated for Si (Z=14, $a_\mathrm{TF} = 0.194$ Å) and Ge (Z=32, $a_\mathrm{TF} = 0.148$ Å) atoms within the Moliére, Pacios and Doyle-Turner approximations, as indicated in the common legend.
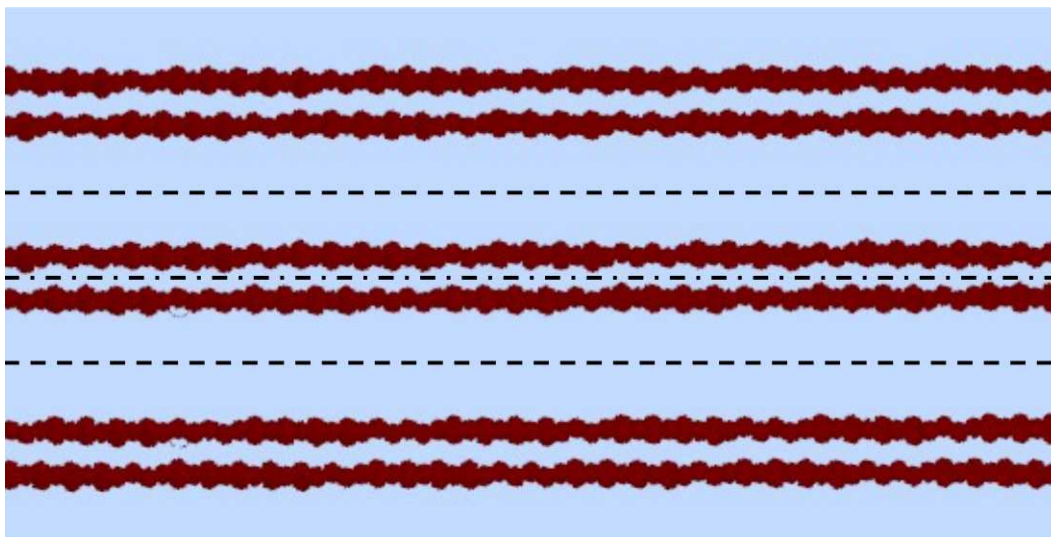

Figure A2. Atoms (red circles) arranged in the (111) planes in a crystal with the diamond cubic crystal structure. Due to thermal vibrations the atoms are shifted from the nodal positions resulting in an uneven profile of the planes. Two dashed lines mark the boundaries of the (111) channel for a negatively charged projectile particle. Dot-dashed line marks the channel's center-line. The figure was rendered using the multitask software toolkit MBNSTUDIO [33].

References

[1] J. Lindhard, Influence of crystal lattice on motion of energetic charged particles. K. Dan. Vidensk. Selsk. Mat. Fys. Medd. **34**, 1 (1965).
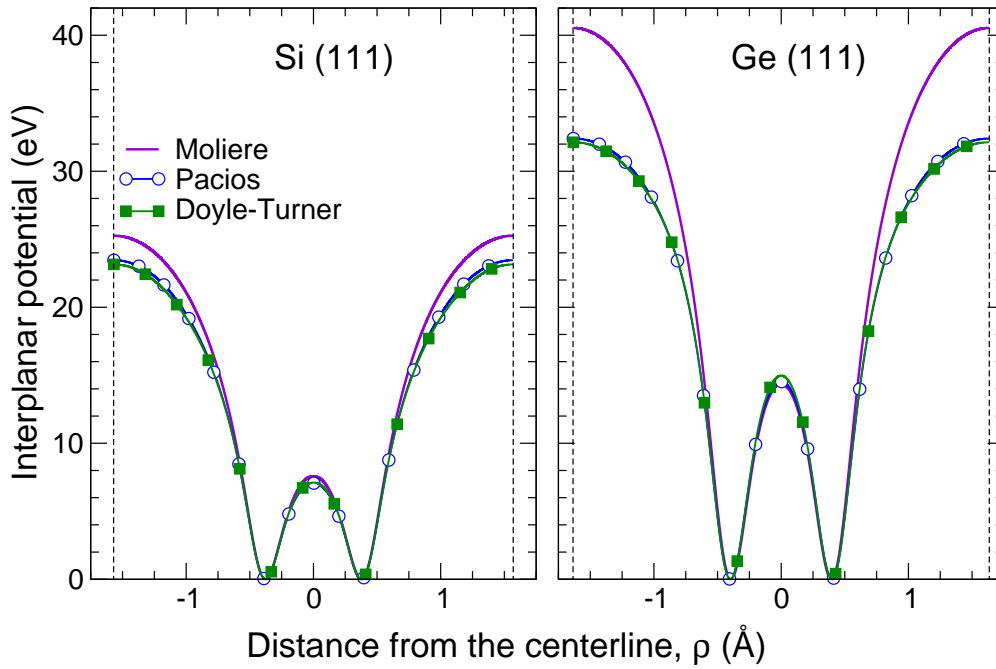
Figure A3. Electron (111) inter-planar potentials $U_{pl}(\rho)$ in silicon (left) and germanium (right) crystals calculated at $T = 300\,^{\circ}\text{C}$ using the Moliére, Pacios and Doyle-Turner approximations.

[2] V. M. Biryukov, Yu. A. Chesnokov, and V. I. Kotov, *Crystal Channeling and Its Application at High-Energy Accelerators.* Springer Science & Business Media (2013).

[3] U. I. Uggerhøj, The interaction of relativistic particles with strong crystalline fields. *Rev. Mod. Phys.* **77**, 1131 (2005).

[4] A. Mazzolari, E. Bagli, L. Bandiera, V. Guidi, H. Backe, W. Lauth, V. Tikhomirov, A. Berra, D. Lietti, M. Prest, E. Vallazza, and D. De Salvador, Steering of a sub-GeV electron beam through planar channeling enhanced by rechanneling. *Phys. Rev. Lett.* **112**, 135503 (2014).

[5] A. Mazzolari, M. Romagnoni, R. Camattari, E. Bagli, L. Bandiera, G. Germogli, , V. Guidi, G. Cavoto, Bent crystals for efficient beam steering of multi TeV-particle beams. Si crystal. *Eur. Phys. J. C* **78**, 720 (2018).

[6] U. Wienands, T. W. Markiewicz, J. Nelson, R. J. Noble, J. L. Turner, U. I. Uggerhøj, T. N. Wistisen, E. Bagli, L. Bandiera, G. Germogli, V. Guidi, A. Mazzolari, R. Holtzapple, and M. Miller, Observation of Deflection of a Beam of Multi-GeV Electrons by a Thin Crystal. *Phys. Rev. Lett.* **114**, 074801 (2015).

[7] W. Scandale, G. Arduini, R. Assmann, C. Bracco, S. Gilardoni, V. Ippolito, E. Laface, R. Losito, A. Masi, E. Metral, V. Previtali, S. Redaelli, M. Silari, L. Tlustos, E. Bagli, S. Baricordi, P. Dalpiaz, V. Guidi, A. Mazzolari et al., First results on the SPS beam collimation with bent crystals. *Phys. Lett.* **692B**, 78-82 (2010).

[8] W. Scandale, G. Arduini, F. Cerutti, M. Garattini, S. Gilardoni, A. Lechner, R. Losito, A. Masi, D. Mirarchi, et al., Focusing of 180 GeV/c pions from a point-like source into a parallel beam by a bent silicon crystal. *Nucl. Instrum. Method B* **446**, 15-18 (2019)

[9] A. V. Korol and A. V. Solov'yov. *Novel Light Sources beyond Free Electron Lasers*, Springer Nature Switzerland AG (2022).

[10] G. B. Sushko, A. V. Korol and A. V. Solov'yov, Extremely brilliant crystal-based light sources, *Europ. Phys. J. D* **76**, 166 (2022).

[11] A. V. Korol and A. V. Solov'yov, Atomistic modeling and characterizaion of light sources based

on small-amplitude short-period periodically bent crystals. *Nucl. Instrum. Methods B* **537**, 1 (2023).

[12] M. A. Kumakhov. On the theory of electromagnetic radiation of charged particles in a crystal. Phys. Lett. **57A**, 17-18 (1976).

[13] V. V. Kaplin and S. A. Vorobiev, On the electromagnetic radiation of channeled particles in a curved crystal. *Phys. Lett.* **67A**, 135 (1978).

[14] A. M. Taratin and S. A. Vorobiev, Radiation of high-energy positrons channeled in bent crystals. *Nucl. Instrum. Meth. B* **31**, 551 (1988).

[15] Korol, A. V., Solov'yov, A. V. and Greiner, W. Coherent radiation of an ultrarelativistic charged particle channeled in a periodically bent crystal. *J. Phys. G: Nucl. Part. Phys.* **24**, L45 (1998).

[16] Andrey V. Korol, Andrey V. Solov'yov, and Walter Greiner. *Channeling and Radiation in Periodically Bent Crystals*, Second Edition. Springer Series on Atomic, Optical, and Plasma Physics **69**, Springer-Verlag, Berlin Heidelberg (2014).

[17] A. V. Korol, G. B. Sushko, A. V. Solov'yov, All-atom relativistic molecular dynamics simulations of channeling and radiation processes in oriented crystals. *Europ. Phys. J. D* **75**, 107 (2021)

[18] H. Backe and W. Lauth, Channeling experiments with sub-GeV electrons in flat silicon single crystals. *Nucl. Instrum. Meth. B* **335**, 24 (2015).

[19] W. Scandale, L. S. Esposito, M. Garattini, R. Rossi, V. Zhovkovska, A. Natochii, F. Addesa, F. Iacoangeli, F. Galluccio, F. Murtas, A. G. Afonin, Yu. A. Chesnokov, A. A. Durum, V. A. Maisheev, Yu. E. Sandomirskiy, A. A. Yanovich, G. I. Smirnov, Yu. A. Gavrikov, Yu. M. Ivanov, M. A. Koznov, M. V. Malkov, L. G. Malyarenko, I. G. Mamunct, J. Borg, T. James, G. Hall, M. Pesaresi, Reduction of multiple scattering of high-energy positively charged particles during channeling in single crystals. *Eur. Phys. J. C* **79**, 99 (2019)

[20] L. Bandiera, E. Bagli, G. Germogli, V. Guidi, A. Mazzolari, H. Backe, W. Lauth, A. Berra, D. Lietti, M. Prest, D. De Salvador, E. Vallazza, and V. Tikhomirov, Investigation of the electromagnetic radiation emitted by sub-GeV electrons in a bent crystal. *Phys. Rev. Lett.* **115**, 025504 (2015)

[21] T. N. Wistisen, U. I. Uggerhøj, U. Wienands, T. W. Markiewicz, R. J. Noble, B. C. Benson, T. Smith, E. Bagli, L. Bandiera, G. Germogli, V. Guidi, A. Mazzolari, R. L. Holtzapple, and S. Tucker, Channeling, volume reflection, and volume capture study of electrons in a bent silicon crystal. *Phys. Rev. Accel. Beams* **19**, 071001 (2016).

[22] E. Bagli, V. Guidi, A. Mazzolari, L. Bandiera, G. Germogli, A. I. Sytov, D. De Salvador, A. Berra, M. Prest, E. Vallazza, Experimental evidence of independence of nuclear de-channeling length on the particle charge sign. *Eur. Phys. J. C* **77**, 71 (2017)

[23] A. I. Sytov, L. Bandiera, D. De Salvador, A. Mazzolari, E. Bagli, A. Berra, S. Carturan, C. Durighello, G. Germogli, V. Guidi, P. Klag, W. Lauth, G. Maggioni, M. Prest, M. Romagnoni, V. V. Tikhomirov, and E. Vallazza, Steering of Sub-GeV electrons by ultrashort Si and Ge bent crystals. *Eur. Phys. J. C* **77**, 901 (2017).

[24] U. Wienands, S. Gessner, M. J. Hogan, T. W. Markiewicz, T. Smith, J. Sheppard, U. I. Uggerhøj, J. L. Hansen, T. N. Wistisen, E. Bagli, L. Bandiera, G. Germogli, A. Mazzolari, V. Guidi, A. Sytov, R. L. Holtzapple, K. McArdle, S. Tucker, B. Benson, Channeling and radiation experiments at SLAC. *Nucl. Instrum Meth. B* **402**, 11 (2017)

[25] L. Bandiera, A. Sytov, D. De Salvador, A. Mazzolari, E. Bagli, R. Camattari, S. Carturan, C. Durighello, G. Germogli, V. Guidi, P. Klag, W. Lauth, G. Maggioni, V. Mascagna, M. Prest, M. Romagnoni, M. Soldani, V. V. Tikhomirov, and E. Vallazza, Investigation on radiation generated by sub-GeV electrons in ultrashort silicon and germanium bent crystals. *Eur. Phys. J. C* **81**, 284 (2021).

[26] H. Backe, D. Krambrich, W. Lauth, K. K. Andersen, J. L. Hansen, U. I. Uggerhøj, Channeling and Radiation of Electrons in Silicon Single Crystals and $Si_{1-x}Ge_x$ Crystalline Undulators. *J. Phys.: Conf. Ser.* **438**, 012017 (2013).

[27] E. Bagli, L. Bandiera, V. Bellucci, A. Berra, R. Camattari, D. De Salvador, G. Germogli, V. Guidi,

L. Lanzoni, D. Lietti, A. Mazzolari, M. Prest, V. V. Tikhomirov, and E. Vallazza, Experimental evidence of planar channeling in a periodically bent crystal, *Eur. Phys. J. C* **74**, 3114 (2014).

[28] T. N. Wistisen, K. K. Andersen, S. Yilmaz, R. Mikkelsen, J. L. Hansen, U. I. Uggerhøj, W. Lauth, and H. Backe. Experimental realization of a new type of crystalline undulator, *Phys. Rev. Lett.* **112**, 254801 (2014).

[29] U. I. Uggerhøj, T. N. Wistisen: Intense and energetic radiation from crystalline undulators, *Nucl. Instrum. Meth. B* **355**, 35 (2015).

[30] I. A. Solov'yov, A. V. Yakubovich, P. V. Nikolaev, I. Volkovets, and A. V. Solov'yov, MesoBioNano Explorer – A universal program for multiscale computer simulations of complex molecular structure and dynamics. *J. Comp. Phys.* **33**, 2412 (2012).

[31] I. A. Solov'yov, A. V. Korol, and A. V. Solov'yov, *Multiscale Modeling of Complex Molecular Structure and Dynamics with MBN Explorer.* Springer International Publishing, Cham, Switzerland (2017).

[32] MBN Explorer and MBN Studio Software at http://mbnresearch.com/software-0

[33] G. B. Sushko, I. A. Solov'yov, and A. V. Solov'yov, Modeling MesoBioNano systems with MBN Studio made easy. *J. Mol. Graph. Model.* **88**, 247 (2019).

[34] D. De Salvador, S. Carturan, A. Mazzolari, E. Bagli, L. Bandiera, C. Durighello, G. Germogli, V. Guidi, P. Klag, W. Lauth, G. Maggioni, M. Romagnoni, and A. Sytov, Innovative remotely-controlled bending device for thin silicon and germanium crystals. *JINST*, **13**, C04006 (2018).

[35] V. V. Haurylavets, A. Leukovich, A. Sytov, L. Bandiera, A. Mazzolari, M. Romagnoni, V. Guidi, G. B. Sushko, A. V. Korol, and A. V. Solov'yov, MBN Explorer atomistic simulations of 855 MeV electron propagation and radiation emission in oriented silicon bent crystal: theory versus experiment, *Eur. Phys. J. Plus* **137**, 34 (2022).

[36] G. B. Sushko, V. G. Bezchastnov, I.A. Solov'yov, A. V. Korol, W. Greiner, and A. V. Solov'yov, Simulation of ultra-relativistic electrons and positrons channeling in crystals with MBN Explorer. *J. Comp. Phys.* **252**, 404 (2013).

[37] G. Molière, Theorie der Streuung schneller geladener Teilchen I: Einzelstreuung am abgeschirmten Coulomb-Feld. *Z. f. Naturforsch* **A2**, 133 (1947).

[38] L. Fernandes Pacios, Analytical Density-Dependent Representation of Hartree-Fock Atomic Potentials. *J. Comp. Chem.* **14**, 410 (1993).

[39] P. A. Doyle and P. S. Turner, Relativistic Hartree-Fock X-ray and Electron Scattering Factors. *Acta Cryst. A* **24**, 390 (1968).

[40] G. B. Sushko, V. G. Bezchastnov, A. V. Korol, Walter Greiner, A. V. Solov'yov, R. G. Polozkov, and V. K. Ivanov, Simulations of electron channeling in bent silicon crystal. *J. Phys. Conf. Ser.* **438**, 012019 (2013).

[41] G. B. Sushko, A. V. Korol, Walter Greiner, and A. V. Solov'yov, Sub-GeV Electron and Positron Channeling in Straight, Bent and Periodically Bent Silicon Crystals. *J. Phys. Conf. Ser.* **438**, 012018 (2013).

[42] R. G. Polozkov, V. K. Ivanov, G. B. Sushko, A. V. Korol, and A. V. Solov'yov, Radiation emission by electrons channeling in bent silicon crystals. *Eur. Phys. J. D* **68**, 268 (2014).

[43] G. B. Sushko, *Atomistic Molecular Dynamics Approach for Channeling of Charged Particles in Oriented Crystals* (Doctoral dissertation), Goethe-Universität, Frankfurt am Main (2015).

[44] Y. Ivanov, A. Petrunin, and V. Skorobogatov, Observation of the elastic quasi-mosaicity effect in bent silicon single crystals. *JETP Lett.* **81**, 977 (2005).

[45] V. Guidi, A. Mazzolari, D. De Salvador, and A. Carnera, Silicon crystal for channelling of negatively charged particles. *J. Phys. D: Appl. Phys.* **42**, 182005 (2009).

[46] R. Camattari, V. Guidi, V. Bellucci, and A. Mazzolari, The quasi-mosaic effect in crystals and its application in modern physics, *J. Appl. Cryst.* **48**, 977 (2015).

[47] H. Backe, P. Kunz, W. Lauth, and A. Rueda, Planar channeling experiments with electrons at the 855 MeV Mainz Microtron MAMI. *Nucl. Instrum. Meth. B* **266**, 3835 (2008).

[48] A. Sytov and V. Tikhomirov, CRYSTAL simulation code and modeling of coherent effects in a

bent crystal at the LHC. *Nucl. Instrum. Methods B* **355**, 383 (2015).

[49] A. M. Taratin and S. A. Vorobiev, Volume trapping of protons in the channeling regime in a bent crystal. *Phys. Lett.* **115A**, 398 (1986).

[50] A. M. Taratin and S. A. Vorobiev, Volume reflection of high-energy charged particles in quasi-channeling states in bent crystals. *Phys. Lett.* **119A**, 425 (1987).

[51] H. Shen, Q. Zhao, F. S. Zhang, G. B. Sushko, A. V. Korol, and A. V. Solov'yov, Channeling and radiation of 855 MeV electrons and positrons in straight and bent tungsten (110) crystals. *Nucl. Instrum. Meth. B* **424**, 26 (2018).

[52] J.D. Jackson, *Classical Electrodynamics* (Wiley, Hoboken, 1999)

[53] http://www.mbnresearch.com/TECHNO-CLS/Main.

[54] G. B. Sushko, A. V. Korol, A. V. Solov'yov, Ultra-relativistic electron beams deflection by quasi-mosaic crystals. *Eur. Phys. J. D* **76**, 236 (2022).